International Journal of Environmental Sciences
ISSN: 2229-7359
Vol. 11 No. 20s, 2025
https://theaspd.com/index.php

Design, Synthesis, And Biological Evaluation Of Some 1,2,4-Triazin-Linked Oxazole Derivatives To Treat Alzheimer's Disease

Omkar Singh[1,2], Vilas B. Ghawate[1,3], Prabhash Nath Tripathi[4], Pravin Kumar Singh[2], Harendra Rai[5], Rajat Rai[2,6]
[1]Bhagawant University, Ajmer - 305004, Rajasthan, India.
[2]Rahul Sankrityayan College of Pharmacy, Azamgarh – 276121, Uttar Pradesh, India.
[3]MES College of Pharmacy, Sonai, Ahmednagar- 414105, Maharashtra, India.
[4]Meerut Institute of Engineering and Technology, Meerut, Uttar Pradesh, India.
[5]Apex Institute of Pharmacy, Mirzapur, Uttar Pradesh, Noida 231304, India
[6]Carreer Point University, Kota – 325003, Rajasthan, India.
Corresponding Author
***Omkar Singh[1,2]**
E-mail: omkarsingh85@gmail.com

Abstract:
Alzheimer's disease (AD) is a complex neurodegenerative disorder characterized by progressive cognitive decline, memory impairment, and synaptic dysfunction. A significant pathological hallmark of AD is the deficiency of cholinergic neurotransmission, primarily caused by excessive activity of acetylcholinesterase (AChE), which degrades acetylcholine in the synaptic cleft.
The compounds were synthesized via a multistep reaction pathway involving the formation of diphenyl-1,2,4-triazine cores followed by condensation with appropriately substituted oxazole moieties. The structural identity of the synthesized compounds was confirmed using spectroscopic techniques, including IR, NMR, and mass spectrometry. All synthesized derivatives were subjected to in vitro AChE inhibition assay using Ellman's method. The results revealed that several compounds demonstrated strong inhibitory activity, with IC_{50} values in the low micromolar range.
In conclusion, the diphenyl-1,2,4-triazin-linked oxazole derivatives presented in this study represent a promising new class of AChE inhibitors for the treatment of AD. Their superior efficacy over oxazole analogs makes them attractive candidates for further development.
Keywords: *Acetylcholine, AChE inhibitors, Chemistry, and Alzheimer's disease*

1. INTRODUCTION

Cognitive function decline, memory loss, and behavioral changes are hallmarks of Alzheimer's disease (AD), a progressive neurological illness that ultimately results in loss of autonomy and death. As of 2023, AD was the leading cause of dementia worldwide, impacting over 55 million people; as the population ages, this number is predicted to quadruple by 2050 [1]. The buildup of β-amyloid (Aβ) plaques and neurofibrillary tangles made of hyperphosphorylated tau protein in the brain is what pathologically characterizes the disease; these eventually cause synaptic dysfunction, neuronal death, and brain atrophy [2].

There are still few and mostly symptomatic treatment options for AD, despite tremendous progress in our understanding of its etiology. Current FDA-approved medications, like NMDA receptor antagonists (memantine) and cholinesterase inhibitors (donepezil, rivastigmine, galantamine), only slightly reduce symptoms and do not stop the progression of the disease [3]. The focus of recent work has been on disease-modifying strategies, such as lecanemab and aducanumab, which are monoclonal antibodies that target β-amyloid. Nevertheless, these therapies are expensive, ineffective, and come with risks such as amyloid-related imaging abnormalities (ARIA) [4]. These drawbacks highlight the urgent need for innovative treatment medicines that more safely and effectively target the underlying processes of AD.

Numerous types of heterocyclic compounds have demonstrated promise in the treatment of neurodegenerative diseases, and their important pharmacological characteristics have long been acknowledged. Three nitrogen atoms make up the six-membered aromatic ring known as the 1,2,4-triazine moiety, which has a variety of biological actions, such as anti-inflammatory, antibacterial, anticancer, and CNS-modulating qualities [5-6]. Its derivatives are good candidates for the creation of anti-Alzheimer drugs since they have been shown to inhibit important enzymes linked to neurodegeneration, including monoamine oxidase (MAO), butyrylcholinesterase (BuChE), and acetylcholinesterase (AChE) [7].

In a similar vein, medicinal chemistry has focused a lot of interest on the oxazole nucleus, a five-membered heterocyclic ring with one nitrogen and one oxygen atom. Numerous biological actions, such as antibacterial, anti-inflammatory, antioxidant, and CNS-related effects, are displayed by oxazole derivatives [8-9]. Several oxazole-based drugs, in particular, have demonstrated promise in blocking AChE, modifying oxidative stress pathways, and shielding neurons from amyloid-induced toxicity—all of which are critical processes in the pathophysiology of AD [10].

One intriguing method to enhance their pharmacological effects is to combine these two heterocyclic moieties—1,2,4-triazine and oxazole—into a single molecular structure. Increased lipophilicity provided by diphenyl-substituted 1,2,4-triazines facilitates improved blood-brain barrier (BBB) penetration, and oxazole rings enhance receptor binding specificity and bioactivity [11].

By connecting these pharmacophores with the right linkers, hybrid compounds can maximize their interactions with various brain targets, which may increase their effectiveness in treating AD [12]. Furthermore, as a unique paradigm in drug discovery for complicated disorders like AD that include numerous pathogenic pathways, multitarget-directed ligands (MTDLs) have gained popularity recently. Since 1,2,4-triazine and oxazole scaffolds may be designed to jointly regulate cholinesterase activity, amyloid aggregation, and oxidative stress, their hybridization is a good fit for the MTDL framework [13]. In order to streamline the design process and cut down on the time and expense of drug development, computational studies like molecular docking and ADMET profiling can help predict pharmacokinetic characteristics and receptor binding affinities [14].

The design, production, and biological assessment of novel diphenyl-1,2,4-triazin-linked oxazole derivatives as possible Alzheimer's disease treatment agents are the main objectives of the current study. The idea is to create compounds that incorporate important pharmacophores that are recognized for their cognitive-boosting and neuroprotective qualities. The goal of this research is to find lead compounds with strong inhibitory action against cholinesterase enzymes, and possible neuroprotective effects using synthetic chemistry, in vitro biological tests and computational studies.

2. RESULTS AND DISCUSSION

2.1. Chemistry

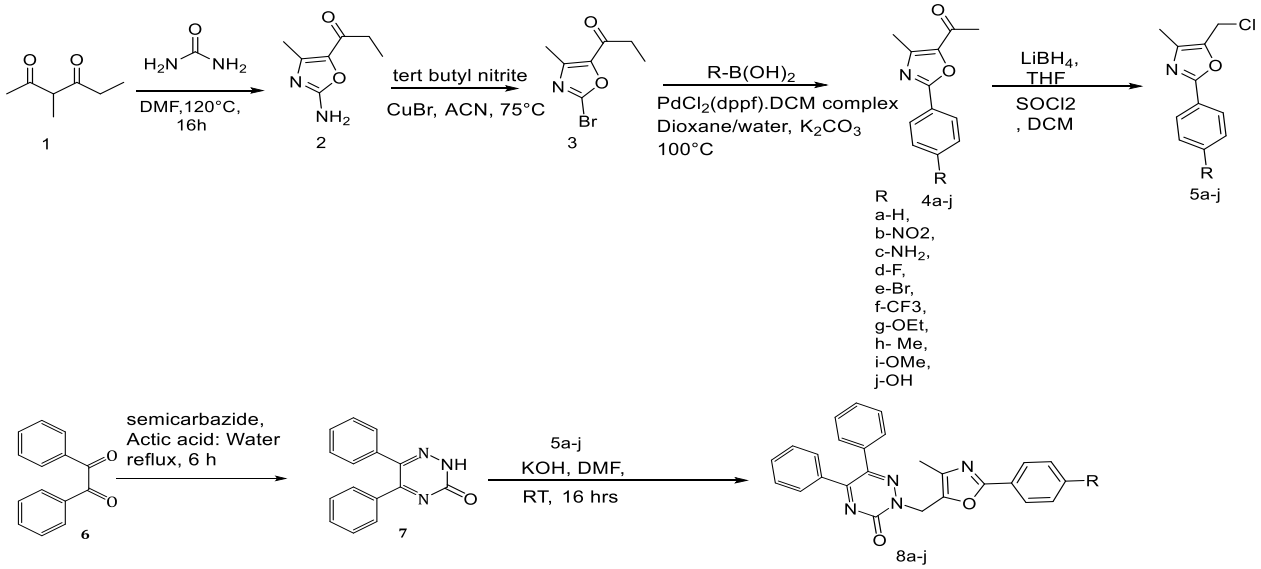

Scheme 1: Synthetic Scheme of the title compounds (8a -8j)**.**

In the first step, 3-methylhexane-2,4-dione (1) is reacted with urea in the presence of DMF to give the 1-(2-amino-4-methylthiazol-5-yl)propan-1-one (2). Then, intermediate (2) is taken into acetonitrile with copper bromide and tertiary butyl nitrile to afford 1-(2-bromo-4-methylthiazol-5-yl)propan-1-one (3). The intermediates (4a-j) were synthesized by the reaction of the intermediate (3) with R-substituted boronic acid, $PdCl_2$(dppf) catalyst and potassium carbonate in dioxane/water. The key intermediate (5a-j) was prepared by the treatment with lithium borohydride solution (2M) in THF followed by thionyl chloride of intermediate (4a-j). These key intermediates (5a-j) were purified by column chromatography to get the pure compounds with 60-84% yield. 5,6- diphenyl-1,2,4-triazine-3-thiol (7) was prepared by the cyclisation reaction of Benzil (6), semicarbazide, in glacial acetic acid. Final compounds (8a-8j) were synthesized by the coupling reaction of intermediate 7 and key intermediates (5a-5j) in the presence of KOH in DMF. UV, I_2 vapours were used to identify the synthesized compounds primarily. The crude products were

purified by recrystallization from ethanol. (FT-IR, ^{1}H NMR and ^{13}C NMR) and elemental analyses were performed for the confirmation of synthesized compounds.

2.2 Biological activity

2.2.1. In vitro Ellman assay:

All the synthesized compounds **(8a–8i)** were evaluated by Ellman's colorimetric method on hAChE (acetylcholinesterase from human erythrocyte) and hBChE (butyrylcholinesterase from human serum) using donepezil as a reference standard (Table 1). The compounds **8b**, **8d, 8e**, **8f**, in this series, which possess electron-withdrawing groups (Nitro, fluro, bromo, trifluoromethyl) on the phenyl ring, exhibited slightly diminished hAChE inhibitory activities compared to those of compounds that possess electron-donating groups. Among all the evaluated derivatives (**8a – 8i**), compound **8i**, bearing an O-methoxy group, displayed the most significant hAChE inhibitory activity (IC_{50} = 1.25 ± 0.59). The enhanced lipophilicity of compound **8i** due to its methoxy group may be the cause of its effective interactions with the active site residues of hAChE. A comparative study between oxazole- and oxazole-linked derivatives was performed to determine the impact of the heterocyclic core on biological activity. Interestingly, oxazole derivatives consistently exhibited superior AChE inhibition compared to other oxazole analogs. This enhanced activity is attributed to the presence of an electronegative oxygen atom in the oxazole ring, which likely facilitates stronger hydrogen bonding and better interaction within the active site of AChE. Compound **8i** only synthesized compounds that significantly inhibited hBChE. Ellman's colorimetric method on hAChE (acetylcholinesterase from human erythrocyte) and hBChE (butyrylcholinesterase from human serum) using donepezil as a reference standard **(Table 1)** was applied for the evaluation of all the synthesized compounds **(8a–8j)**.

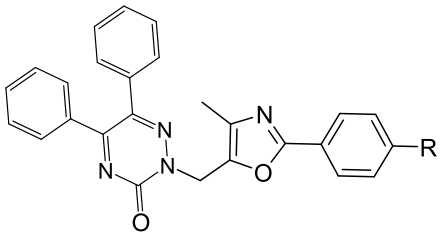

S. No	R	Compound code	hAChE IC_{50} ± SDM (µM)	hBChE IC_{50} ± SD (µM)	[a]SI ratio
1	4-H	**8a**	>100	40.78 ± 5.24	-
2	4-NO_2	**8b**	5.91 ± 0.43	>100	-
3	4-NH_2	**8c**	>100	>100	-
4	4-F	**8d**	>100	25.74 ± 5.82	-
5	4-Br	**8e**	6.57 ± 1.53	31.57 ± 1.51	4.80
6	4-CF_3	**8f**	15.27 ± 2.78	>100	-
7	4- OEt	**8g**	>100	>100	-
8	4-Me	**8h**	5.08 ± 2.56	15.69 ± 1.25	3.08
9	4-OMe	**8i**	1.25 ± 0.59	6.43 ± 0.28	5.14
10	4-OH	**8j**	>50	>100	-
11	Donepezil		0.20 ± 0.01	-	-

[a]Selective index ratio = (hBChE IC_{50})/(hAChE IC_{50})

2.2.2. Acute toxicity study:

Healthy Swiss albino mice (25–30 g) were taken for an acute toxicity study of compound **8i** following the OECD 423 guidelines. Monitoring for Several behavioural changes, cholinergic effects and toxic reactions, such as tremors, convulsions, salivation, diarrhoea, sleep, lacrimation, and feeding behaviour, was done. After administration of test compound **8i**, no signs of any cholinergic side effects, or any toxicity or mortality were observed, a significant safety margin has been shown by compound **8i**.

2.2.3. In vivo Scopolamine-induced Y-maze-based memory study

Compound **8i** was assessed for its ability to enhance learning and memory against a scopolamine-induced cognitive deficit. The results showed a significantly decreased spontaneous alternation rate in scopolamine compared to the control. Treatment with compound **8i** elicited a dose-dependent increase (2.5 mg/kg: < 5 and 10 mg/kg) in the spontaneous alternation rate compared to scopolamine **(Fig. 2)**. Additionally, the

locomotive behaviour of the scopolamine-treated mice did not change as confirmed by the nonsignificant changes in total arm entries among all groups (**Fig. 3**). Effect of compound **8i** (2.5, 5 and 10 mg/kg) in the Y-maze test. (A) Spontaneous alterations rate; (B) Number of arm entries; Bars display values as mean ± SD (n=6) and analysed by one-way ANOVA followed by Tukey's test; $p < 0.05$.

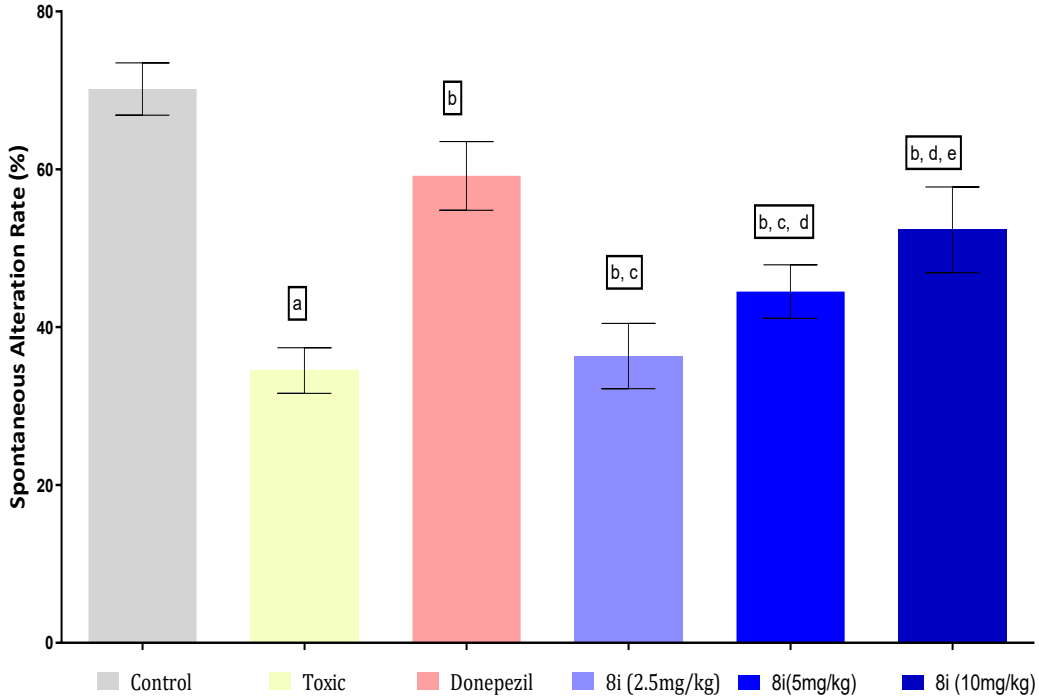

Figure 2 . Spontaneous alternation rate compared to scopolamine

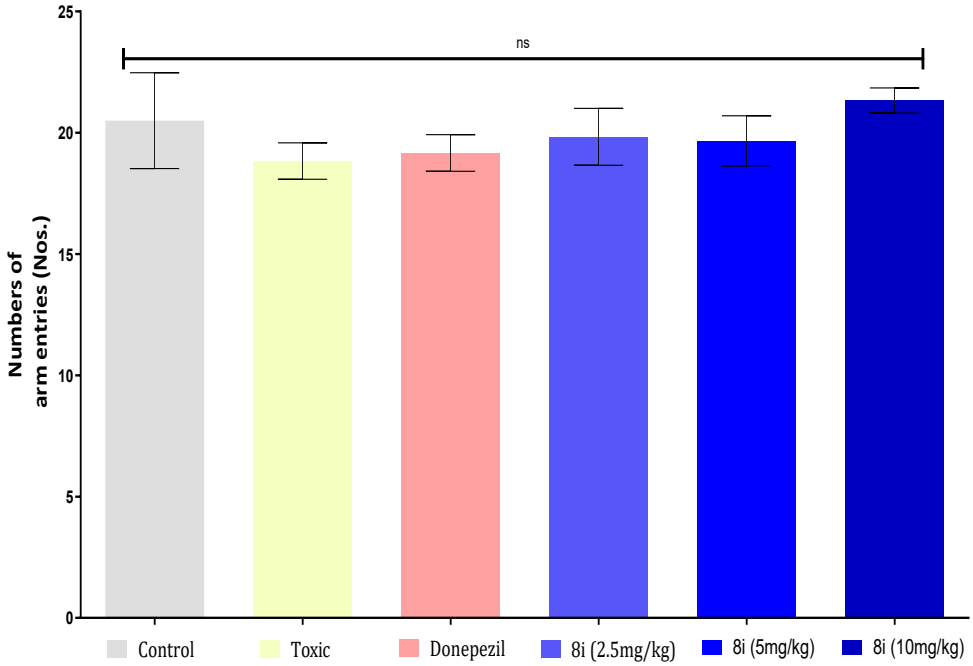

Figure 3. Non-significant changes in total arm entries among all groups.

2.3. Computational studies

2.3.1. Molecular docking

Glide module of Schrödinger Maestro 2018–1 was used to assess the binding affinity and pose stability of Compound **8i** in the active sites of hAChE (PDB Code: 4EY7) for a molecular docking study. For validation of the docking parameters, the crystallized Aricept (donepezil) ligand was extracted and re-docked in the hAChE grid. In the comparative study of the poses of the crystallized and redocked ligands using a superposition tool RMSD value was found to be 0.2 Å.

International Journal of Environmental Sciences
ISSN: 2229-7359
Vol. 11 No. 20s, 2025
https://theaspd.com/index.php

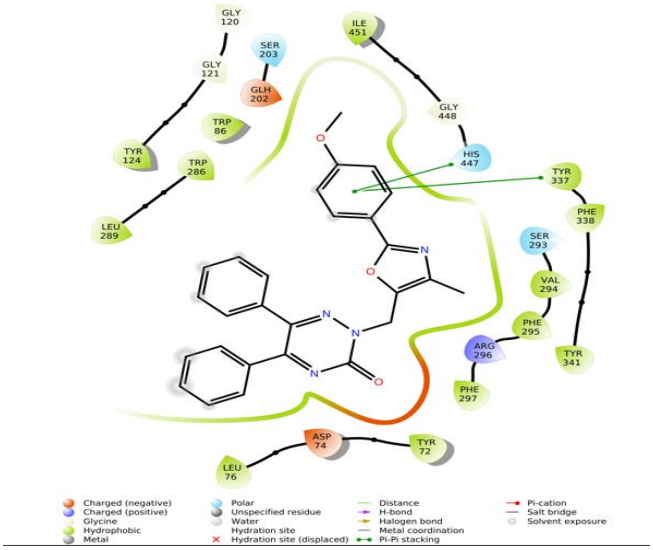

Figure 4. Docking pose of compound 8i with hAChE.

Docked scores were found to be -9.878 kcal/mole for donepezil and −14.6 kcal/mole for Compound **8i**. π-π stacking and polar interactions with His447 in the catalytic active site (CAS) were observed by the methoxy group of Compound **8i**.

All PAS residues were interacted with by Compound **8i** through hydrophobic interactions (Tyr72, Tyr124, Trp286, and Tyr341) and electrostatic interactions (Asp74). Hydrophobic interactions with Trp86 and Phe338 and electrostatic interactions with the Glu202 residue were formed by Compound **8i** at the anionic subsite. Compound **8i** interacted with Gly121 and Gly122 and formed hydrophobic interactions with Ala204 at the oxyanion site **(Fig. 4)**.

2.3.2. Molecular dynamics study

A 100 nsec MD simulation was performed to affirm the binding pose stability of the Compound **8i-hAChE** docked complex. The generated trajectories were utilized to produce simulation interaction diagrams, and the results were analyzed. The stability of the docked protein–ligand complex was determined by RMSD (root mean square deviation) and RMSF (root mean square fluctuation) calculations. The protein–ligand RMSD showed initial fluctuations up to 40 nsec before stabilizing. The docked complex was compared to the reference protein backbone structure, which was stabilized and found to be within 1–3 Å. The structural stability of the protein and Compound **8i** was also evaluated based on the RMSF value, which was found to be < 3 Å and confirming the absence of overall local changes along the protein chain and positions of the atoms in the ligand **(Fig. 5)**.

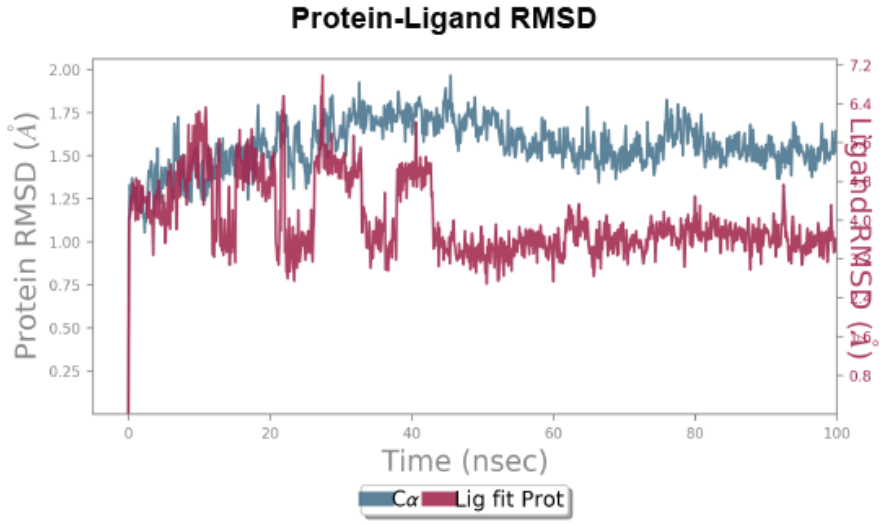

Figure 5. Protein-Ligand RMSD of compound 8i and hAChE.

The results of the MD simulations were analyzed using simulation interaction diagrams. The representation of the interaction analysis through stacked bar charts showed the normalized value of the interaction fractions over the course of the trajectory. The detailed analysis showed that Compound **8i**

interacted through H bonding, hydrophobic interactions and salt-bridge formation with Tyr72, Asp74, Tyr124, Trp337 and Tyr341 in the PAS with interaction fractions of 0.52, 0.68, 0.69, 0.74 and 0.81, respectively. Furthermore, interaction analysis was represented graphically (**Fig. 6**) to show the H-bonding and hydrophobic interactions that existed for more than 20% of the total simulation run time.

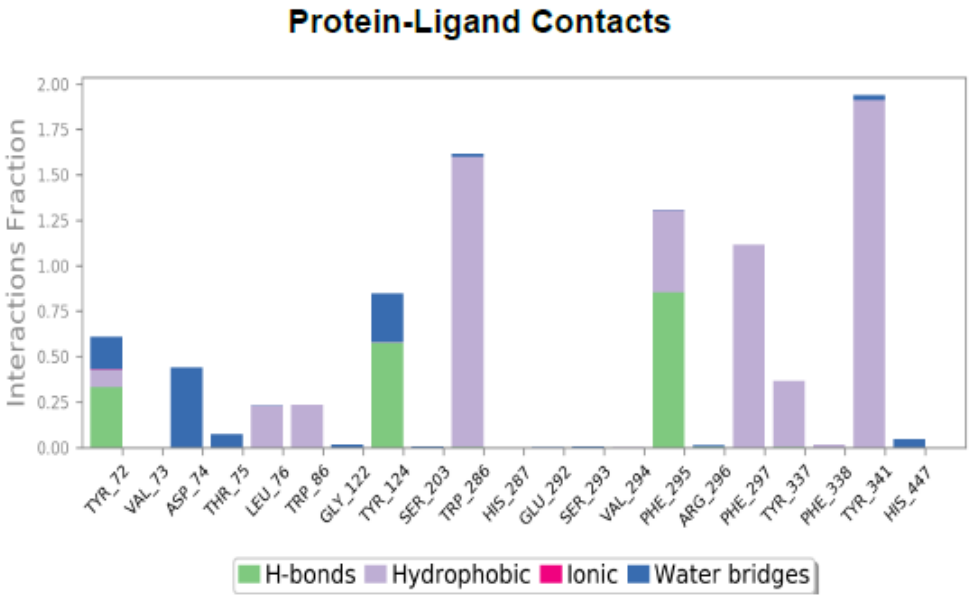

Figure 6. Interaction analysis of compound 8i and hAChE.

The results showed that the nitrogen atom of 2-AP exhibited H-bonding interactions with Asp74 (20%) and Trp337 (22%) at the PAS. Additionally, Asp74 showed H-bonding interactions (21%) with the –NH linker. Furthermore, the results suggested a hydrophobic interaction between Compound **8i** and the Tyr341 residue at the PAS. The results of the MD simulation analysis were also analyzed as a function of time (**Fig. 7**). The top panel of a timeline representation shows the total number of specific contacts (H-bonding, hydrophobic, ionic, and water bridge interactions) between the protein and the ligand over the course of the simulation run. The bottom panel shows the interactions of individual amino acid residues in each trajectory frame during the simulation run. Some residues formed more than one specific interaction with the ligand, which was represented by a darker shade of orange according to the scale at the right of the plot. Overall, the results of the MD simulation analysis suggested stable and effective interactions between Compound **8i** and the PAS, and the results were found to agree with in vitro and i

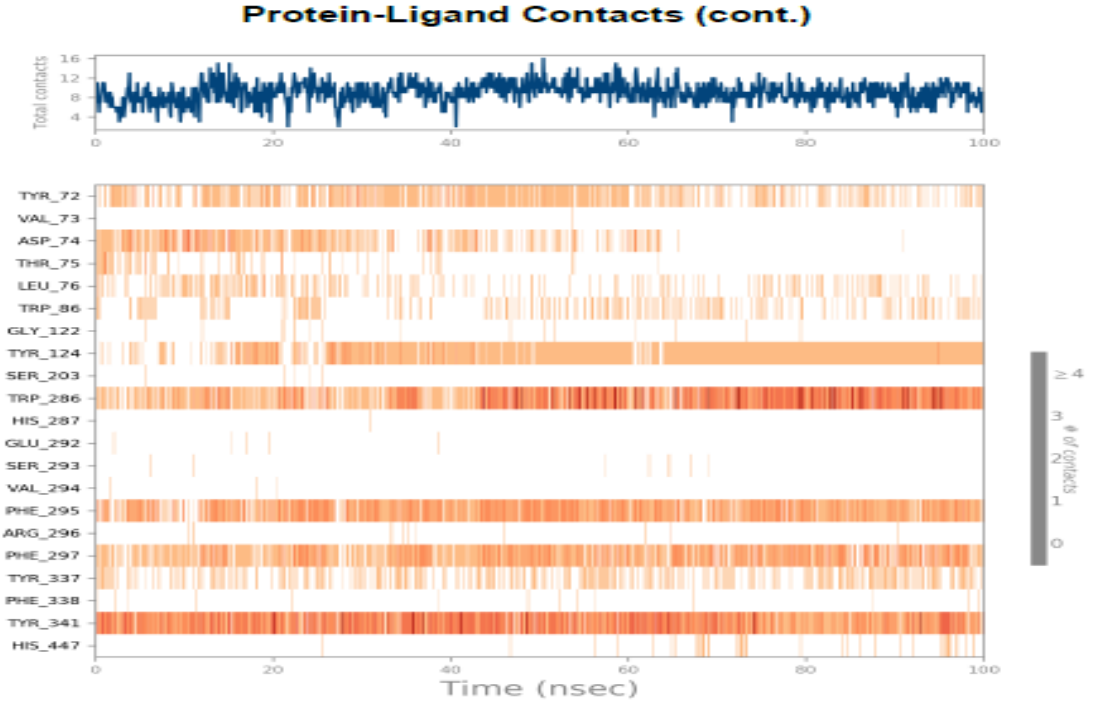

n vivo assays.

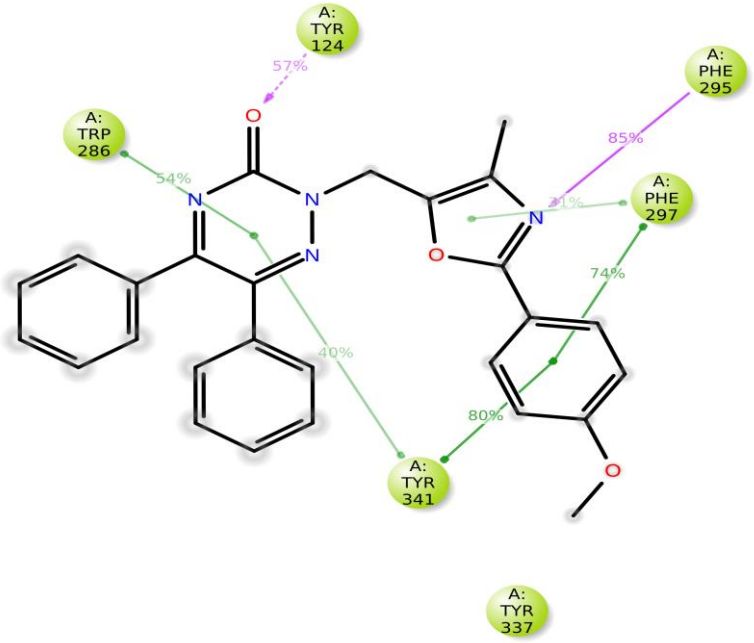

Figure 7. The timeline representation shows the total number of specific contacts of compound 8i and hAChE.

3. CONCLUSION:

Herein, we designed and synthesized a novel set of multitarget-directed molecules with both a triazine moiety and a substituted 1,3,4-oxazole ring for the treatment of cognitive dysfunctions. Among all the synthesized derivatives, the methoxy group-bearing compound **8i** showed the highest in vitro hAChE inhibitory activity (IC_{50}=1.25). In vivo behavioral studies revealed that compound 8d (10mg/kg) significantly reversed the scopolamine-induced cognitive dysfunctions in mice as evaluated by Y-maze and passive avoidance tests. Computational studies corroborated the pharmacological outcomes owing to the effective interactions between compound **8i** and the active site residues of PAS. Thus, this study indicated that multi-targeted 5,6- diphenyl-1,2,4-triazine-3-oxazole derivatives are potential scaffolds for the treatment of dementia, with compound **8i** as a promising lead for further research.

4. Experimental section

4.1. Chemistry:

All the chemicals and reagents were obtained from Sigma-Aldrich (India), Cayman chemicals (USA), Avra Synthesis (India) and were utilized without purifying until stated. The melting points were calculated on Stuart melting point apparatus (SMP10) using capillary tubes and are reported as uncorrected. The reaction progress was monitored using a pre-coated silica G60 aluminum sheet (Merck, Germany) using n-hexane/ Ethyl acetate (EtOAc) (80:20 v/v) as mobile phase, followed by TLC visualization accomplished on UV light with various visualizing agents i.e., Dragendorff's reagent, and/or iodine vapors. Merck silica gel was employed for column chromatography. 1H and 13C NMR spectra were documented using DMSO-d6 as a solvent on a 500 MHz FT NMR spectrophotometer (Bruker, USA). Mass spectra were recorded on an X500R QTOF (Applied Biosystems) mass spectrometer in positive ion mode.

4.1.1. General procedure of synthesis of (5a-j)

3-methylhexane-2,4-dione (**1**) was reacted with thiourea in the presence of DMF at 120°C for 16 h to give the 1-(2-amino-4-methylthiazol-5-yl)propan-1-one (**2**). Then, intermediate (**2**) is taken into acetonitrile with copper bromide and tertiary butyl nitrile at 75°C for 4-5 h to afford the 1-(2-bromo-4-methylthiazol-5-yl)propan-1-one (**3**). The compound (**3**) reacted with the R-substituted boronic acid and potassium carbonate in the presence of dioxane/water under nitrogen. Added PdCl2(dppf).DCM complex catalyst at 100°C for 16 h to afford (**4a-j**). The compound (**4a-j**) is treated with lithium borohydride solution (2M) in the presence of THF solvent. Quenched reaction with ice-cold water and extracted with ethyl acetate to afford crude compound, which was further treated with thionyl chloride in the presence of 0°C for 2 h to afford intermediate (**5a-j**). These final compounds were purified by column chromatography to get the pure compounds with 60-84% yield. Further, the synthesized derivatives were established using the state of art spectroscopy.

Compound 1: Yield: 5.27g; 87.82%; ^{1}H-NMR shifts (DMSO-d_6, δ ppm): 3.30 (q, 1H), 2.45 (q, 2H), 2.29 (s, 3H), 1.04 (t, 3H), 0.78 (s, 3H). LCMS: 95%.
Compound 2: Yield: 4.0 g; 75%; 1HNMR (400 MHz, DMSO-d_6), δ- 6.99 (s, 2H), 3.40 (qt, J = 8.0 Hz, 2H), 2.45 (s, 3H), 1.18 (t, J = 7.6 Hz, 3H). LCMS: 90%.
Compound 3: Yield: 3.0 g; 87.82%; 1HNMR (400 MHz, DMSO-d6), δ- 3.39 (qt, J = 8.0 Hz, 2H), 2.44 (s, 3H), 1.17 (t, J = 7.6 Hz, 3H). LCMS: 90%.
Compound 4a: Yield: 3.5 g; 70%; 1HNMR (400 MHz, DMSO-d6), δ - 7.67 – 7.30 (m, 5H), 3H), 2.45 (s, 3H), 2.19 (s, 3H). LCMS: 90%.
Compound 4b: Yield: 3.0g; 87.82%; 1HNMR (400 MHz, DMSO-d6), δ - 7.51 – 7.25 (m, 4H), 3H), 2.45 (s, 3H), 2.19 (s, 3H). LCMS: 91%.
Compound 4c: Yield: 2.8 g; 87.82%; 1H-NMR shifts (DMSO-d6, δ ppm): 8.12 – 7.78 (m, 2H), 7.10 - 7.30 (m, 2H), 5.10 (s, 2H), 2.35 (s, 3H), 1.90 (t, 3H). LCMS: 85%.
Compound 4d: Yield: 2.5 g; 87.82%; 1H-NMR shifts (DMSO-d6, δ ppm): 8.12 – 7.57 (m, 4H), 2.35 (s, 3H), 1.20 (t, 3H). LCMS: 86%. ^{13}C-NMR shifts (DMSO-D6-D6, δ ppm): 7.5, 16.9, 31.9, 115.0, 130.5, 141.2, 144.2, 145.9, 164.4, 169.5, 198.5
Compound 4e: Yield: 2.4 g; 87.82%; 1H-NMR shifts (DMSO-d6, δ ppm): 8.12 – 7.78 (m, 4H), 2.35 (s, 3H), 1.80 (t, 3H). LCMS: 80%.
Compound 4f: Yield: 2.0 g; 87.82%; 1H-NMR shifts (DMSO-d6, δ ppm): 7.78 – 7.10 (m, 4H), 2.40 (s, 3H), 1.51 (t, 3H). LCMS: 80%.
Compound 4g: Yield: 1.0 g; 87.82%; 1H-NMR shifts (DMSO-d6, δ ppm): 7.50 – 7.10 (m, 4H), 3.80 (q, J = 7.12 Hz, 2H), 2.38 (s, 3H), 2.10 (s, 3H), 1.25 (t, 3H). LCMS: 85%.
Compound 4h: Yield: 1.0 g; 87.82%; 1H-NMR shifts (DMSO-d6, δ ppm): 7.80 – 7.10 (m, 4H), 3.90 (q, J = 7.0 Hz, 2H), 2.30 (s, 3H), 1.91 (s, 3H), 1.25 (t, 3H). LCMS: 80%.
Compound 4i: Yield: 1.0 g; 87.82%; 1H-NMR shifts (DMSO-d6, δ ppm): 8.31 – 7.10 (m, 4H), 3.75 (s, 3H), 2.30 (s, 3H), 1.90 (t, 3H). LCMS: 75%.
Compound 4j: Yield: 1.2 g; 87.82%; 1H-NMR shifts (DMSO-d6, δ ppm): 8.85 (s, 1H), 7.70 – 7.10 (m, 4H), 2.40 (s, 3H), 2.10 (s, 3H). LCMS: 80%.
Compound 5a: Yield: 500 mg; 87.82%; 1H-NMR shifts (DMSO-d6, δ ppm): 8.10 – 7.50 (m, 5H), 4.67 (s, 2H) 2.25 (s, 3H), LCMS: 90%, ^{13}C-NMR shifts (DMSO-d6, δ ppm): 14.5, 42.8, 128.6, 129.8, 130.6, 143.9, 152.4, 169.2
Compound 5b: Yield: 400 mg; 87.82%; 1H-NMR shifts (DMSO-d6, δ ppm): 8.10 – 7.65 (m, 4H), 4.67 (s, 2H) 2.25 (s, 3H). LCMS: 90%, ^{13}C-NMR shifts (DMSO-d6, δ ppm): 14.9, 42.5, 115.3, 129.1, 129.4, 133.3, 145.6, 152.0, 167.6
Compound 5c: Yield: 300 mg; 87.82%; 1H-NMR shifts (DMSO-d6, δ ppm): 7.80 – 6.75 (m, 4H), 5.25 (brs, 2H) 4.60 (s, 2H), 2.20 (s, 3H). LCMS: 90%, ^{13}C-NMR shifts (DMSO-d6, δ ppm): 14.9, 42.6, 115.3, 129.9, 130.1, 133.2, 144.8, 153.1, 168.6
Compound 5d: Yield: 350 mg; 87.82%; 1H-NMR shifts (DMSO-d6, δ ppm): 8.78 – 7.78 (m, 4H), 4.51 (s, 2H), 2.20 (s, 3H). LCMS: 90%, ^{13}C-NMR shifts (DMSO-d6, δ ppm): 14.9, 42.6, 116.3, 129.9, 130.1, 138.2, 151.8, 162.9, 168.4
Compound 5e: Yield: 300 mg; 87.82%; 1H-NMR shifts (DMSO-d6, δ ppm): 8.75 – 7.70 (m, 4H), 4.51 (s, 2H), 2.20 (s, 3H). LCMS: 90%, ^{13}C-NMR shifts (DMSO-d6, δ ppm): 14.9, 42.6, 123.1, 129.2, 129.9, 131.1, 142.2, 152.0, 168.5
Compound 5f: Yield: 300 mg; 87.82%; 1H-NMR shifts (DMSO-d6, δ ppm): 7.97 - 7.05 (m, 4H), 4.51 (s, 2H), 2.10 (s, 3H). LCMS: 90%, ^{13}C-NMR shifts (DMSO-d6, δ ppm): 14.5, 42.6, 124.1, 125.8, 127.9, 129.2, 129.9, 131.1, 146.3, 152.1, 168.7
Compound 5g: Yield: 300 mg; 87.82%; 1H-NMR shifts (DMSO-d6, δ ppm): 8.15 - 7.19 (m, 4H), 4.65 (s, 2H), 4.10 (m, 2H), 2.21(s, 3H), 1.10 (m, 3H). LCMS: 90%, ^{13}C-NMR shifts (DMSO-d6, δ ppm): 14.5, 42.6, 55.8, 114.1, 128.8, 129.2, 135.7, 152.1, 160.6, 168.8
Compound 5h: Yield: 300 mg; 87.82%; 1H-NMR shifts (DMSO-d6, δ ppm): 7.80 - 7.21 (m, 4H), 4.45 (s, 2H), 2.35 (s, 3H), 2.21 (s, 3H). LCMS: 90%, ^{13}C-NMR shifts (DMSO-d6, δ ppm): 14.5, 21.3, 42.6, 127.5, 129.2, 131.7, 140.5, 152.1, 168.8
Compound 5i: Yield: 350 mg; 87.82%; 1H-NMR shifts (DMSO-d6, δ ppm): 7.80 - 7.08 (m, 4H), 4.65 (s, 2H), 3.70 (s, 3H), 195 (s, 3H). LCMS: 90%, ^{13}C-NMR shifts (DMSO-d6 δ ppm): 14.3, 14.8, 42.6, 64.8, 114.6, 128.1, 129.2, 134.9, 140.5, 152.0, 159.4, 168.8

Compound 5j: Yield: 350 mg; 87.82%; 1H-NMR shifts (DMSO-d6, δ ppm): 9.67 (brs, 1H), 7.60 - 7.10 (m, 4H), 4.65 (s, 2H), 2.35 (s, 3H), 2.10 (s, 3H). LCMS: 90%, ^{13}C-NMR shifts (DMSO-d6, δ ppm): 14.3, 42.5, 114.6, 128.1, 129.2, 134.9, 152.0, 159.4, 168.8

4.1.2. General procedure of synthesis of 5,6-diphenyl-1,2,4-triazine-3-thiol (6):

5,6- diphenyl-1,2,4-triazine-3-thiol (**7**) was prepared with minor variations to the previously described procedure. Benzil (**6**) (6g, 28.5 mmol) was dissolved in glacial acetic acid (150 ml) and then added to a hot water (100 ml) mixture of thiosemicarbazide (2.59g, 28.5 mmol) and further reflux for 4 h. The precipitate obtained was recrystallized with ethanol to obtain orange-yellow color crystals of the desired compound. Yield: 5.27g; 87.82%; 1H-NMR shifts (DMSO-d6, δ ppm): 7.31-7.67 (m, 10H). 11.81 (b, NH, 1H); LCMS: 95%, ^{13}C-NMR shifts (DMSO-d6, δ ppm): 179.28, 160.76, 146.67, 132.24, 130.31, 130.13, 129.88, 129.43, 128.75, 128.66, 128.44.

4.1.3. General procedure of synthesis of ethyl 4,5-diphenyl-2H-imidazole-2-carboxylate (7a-j):

Compound (**7**) reacted with oxazole derivatives (**5a-j**) in the presence of Cs_2CO_3 and using catalyst palladium acetate/xanthphos in the presence of 1,4-dioxane solvent at 120°C for 16 h. TLC monitored the reaction mixture, and after completion, the reaction was quenched with water and extracted with ethyl acetate. Combine the organic layer and wash with saturated brine solution. Purified by column chromatography in 100-200 silica gel with 0-50% ethyl acetate in hexane to afford (**8a-j**).

Compound 7: 1H-NMR (400 MHz, DMSO-d6), δ- 16.8 (brs, 1H), 7.43-7.98 (m, 6H). LCMS: 80%.

Compound 8a: Yield: 400 mg; 87.82%; 1H-NMR (400 MHz, DMSO-d6), δ- 8.09 (d, J = 7.5 Hz, 2H), 7.83 (d, J = 7.6 Hz, 4H), 7.53-8.44 (m, 9H), 4.19 (s, 2H), 2.17 (s, 3H). LCMS: 80%.

Compound 8b: Yield: 300 mg; 87.82%; 1H-NMR (400 MHz, DMSO-d6), δ- 8.33 (d, J = 7.5 Hz, 2H), 8.23 (d, J = 7.5 Hz, 2H), 7.79 (d, J = 7.6 Hz, 4H), 7.53-7.44 (m, 6H), 4.19 (s, 2H), 2.17 (s, 3H). LCMS: 90%.

Compound 8c: Yield: 250 mg; 87.82%; 1-NMR (400 MHz, DMSO-d6), δ- 7.79 (d, J = 7.6 Hz, 2H), 7.53-7.42 (m, 10H), 6.59 (d, J = 7.6 Hz, 2H), 4.19 (s, 2H), 2.18 (s, 3H). LCMS: 91%.

Compound 8d: Yield: 200 mg; 87.82%; 1H-NMR (400 MHz, DMSO-d6), δ- 8.29 (t, J = 5.0 Hz, 2H), 7.79 (d, J = 7.6 Hz, 2H), 7.53 (d, J = 7.6 Hz, 4H), 7.47 (d, J = 7.6 Hz, 2H), 7.43 (m, 2H), 7.34 (m, 2H), 4.21 (s, 2H), 2.18 (s, 3H). LCMS: 95%. ^{13}C-NMR shifts (DMSO-d6, δ ppm): 15.3, 32.7, 116.7, 127.8, 128.9, 129.9, 135.5, 136.2, 138.5, 150.3, 152.1, 157.3, 162.3, 168.9, 170.7.

Compound 8e: Yield: 200 mg; 87.82%; 1H-NMR (400 MHz, DMSO-d6), δ- 7.81 (d, J = 7.6 Hz, 2H), 7.68-7.66 (dd, J = 7.6 Hz, 4H), 7.53 (d, J = 7.6 Hz, 4H), 7.51 (d, J = 7.6 Hz, 2H), 7.43 (m, 2H), 4.19 (s, 2H), 2.18 (s, 3H). LCMS: 94%.

Compound 8f: Yield: 200 mg; 87.82%; 1H-NMR shifts (DMSO-d6, δ ppm): 7.27-7.95 (m, 10H), 4.25 (s, 2H), 2.23 (s, 3H), LCMS: 91%. ^{13}C-NMR shifts (DMSO-d6, δ ppm): 14.4, 32.7, 123.6, 125.7, 127.6, 128.7, 129.7, 135.9, 138.5, 146.3, 150.4, 152.1, 156.3, 168.9, 170.9

Compound 8g: Yield: 200 mg; 87.82%; 1H-NMR shifts (DMSO-d6, δ ppm): 7.04-8.17 (m, 10H), 4.22 (s, 2H), 3.84 (s, 3H), 2.24(s, 3H). LCMS: 90%. ^{13}C-NMR shifts (DMSO-d6, δ ppm): 14.5, 32.7, 58.9, 114.9, 127.9, 128.9, 129.9, 136.2, 139.3, 150.1 152.3, 157.0, 160.9, 168.8, 170.9

Compound 8h: Yield: 100 mg; 87.82%; 1H-NMR shifts (DMSO-d6, δ ppm): 7.22-7.97 (m, 10H), 4.24 (s, 2H), 2.37 (s, 3H), 2.23 (s, 3H). LCMS: 90%. ^{13}C-NMR shifts (DMSO-d6, δ ppm): 14.3, 21.3, 32.5, 127.4, 127.7, 128.4, 129.5, 138.3, 140.4, 150.1, 152.1, 156.0, 168.6, 170.8.

Compound 8i: Yield: 100 mg; 87.82%; 1H-NMR shifts (DMSO-d6, δ ppm): 7.03-8.15 (m, 10H), 4.21 (s, 2H), 4.05 (q, 2H), 2.34 (s, 3H), 2.21 (s, 3H), 1.34 (t, 3H). LCMS: 90%. ^{13}C-NMR shifts (DMSO-d6, δ ppm): 14.5, 14.8, 32.5, 64.5, 114.9, 127.6, 128.5, 128.6, 129.5, 134.9, 135.9, 138.5, 150.4, 156.2, 159.6, 168.8, 170.9.

Compound 8j: Yield: 50 mg; 87.82%; 1H-NMR shifts (DMSO-d6, δ ppm): 9.65 (brs, 1H), 6.89-7.84 (m, 10H), 4.25 (s, 2H), 2.25 (s, 3H), LCMS: 90%. ^{13}C-NMR shifts ($CDCl_3$, δ ppm): 14.5, 32.5, 114.9, 127.4, 128.2, 129.6, 135.9, 138.5, 150.6, 152.7, 156.7, 159.4, 168.8, 170.7.

4.2. Biological activity

4.2.1. In vitro Ellman assay

Ellman's assay procedure was used to evaluate the AChE level [15-20]. To start the reaction, first, 25µL of supernatant, 150µL of 0.1M sodium phosphate buffer (pH 7.4), and 100µL of 1mM DTNB to a 96-well microplate. After 10 minutes of fermentation, added 20µL of 7.5mM ATCI. At 412 nm, the reaction mixture's absorbance was measured. The substrate hydrolyzed/min/mg protein was used to express the AChE inhibitory potency results [21-23].

4.2.2. Acute oral toxicity study

In healthy Swiss albino mice, the substance **8i** had been evaluated for acute oral toxicity according with OECD-423, 2001 criteria. The mice received doses of up to 500 mg/kg of the chemical (6g), and they were monitored for adverse responses or death for a total of 14 days [24-28]. The institutional animal ethical committee duly permitted the study protocols and quantity of mice (IAEC/MIET/CPCSEA/01/2025/309).

4.2.3. Y-maze test

The y-maze apparatus is a three-arm maze that is often used for determining mice short-term and instantaneous working memory. Scopolamine hydrobromide was given through the abdomen (i.p.) to all mouse groups except the control group 30 minutes after the seventh day of therapy. For five minutes, the mice in each group were housed in the middle of the y-maze to reconnoiter the three arms. In order to capture the total number of arm entries, activities were monitored in the camera. The formula for calculating the "memory improvement score" is % alternations = (number of alternations/ (total arm entries–2)) ×100[29-35].

4.2.4. Computational Studies:

4.3.1. Molecular docking

The study of compound **8i** consensual binding and active site interactions on hAChE (PDB Code: 4EY7) was done by molecular docking studies. The Protein Preparation Wizard program was used to create the protein's crystal structure. First, bond ordering and hydrogen bonds were assigned. Prime was used to add the missing side chains and loops. Using the Epik at pH 7.0 ± 2.0, the heteroatom states were created and the water molecules that were more than 5Å away from the heteroatoms were eliminated. The protein structure was also optimized using the PROPKA method at pH 7.0 and minimized at restrained minimization by maintaining the convergence heavy atoms RMSD at 0.30Å. The generated protein structure was utilized for receptor grid generation in order to identify the active sites around the distance of 10 x 10 x 10 Å from the centroid of the co-crystallized ligand (donepezil). The stable conformers of ligands (compound **8i** and donepezil) were created using the LigPrep module, and these were then docked using the Glide XP module of Schrödinger Maestro 2018-1. The Glide XP visualizer tool was used to conduct detailed interaction analyses [36-38].

4.3.2. Molecular dynamics

To confirm the binding stability and pattern of the compound **8i**-AChE complex utilizing Desmond, a 100-nsec molecular dynamics simulation run was conducted. The system was first constructed using the system builder, which used a cubic simulation box of the TIP3P explicit water system to create a virtual water environment. The box wall and the protein–ligand complex had to be at least 10Å apart. The system had been neutralized by adding counter ions, and 0.15M NaCl was added to create an isosmotic salt environment. The system's energy was minimized by using a conjugate gradient algorithm with a maximum of 2000 interactions and a convergence criterion of 1 kcal/mol/Å. The system's temperature and pressure were set to 300K and 1.013 atmospheric bar, respectively, and a 100 nsec simulation run with periodic boundary conditions under an isothermal-isobaric ensemble (NPT) was performed out subsequent energy reduction [39-41].

REFERENCES:

1. Geronikaki AA, Dearden JC, Filimonov D, et al. J Med Chem. 2004;47(11):2870–2876.
2. Piplani P, Danta CC. Bioorg Chem. 2015;60:64–73.
3. Guillozet AL, Weintraub S, Mash DC, Mesulam MM. Arch Neurol. 2003;60(5):729–736.
4. Tham W, Auchus AP, Thong M, Goh M-L, Chang H-M, Wong M-C. Chen CP-H. J Neurol Sci. 2002;203:49–52.
5. Tyler CR, Allan AM. Curr Environ Health Rep. 2014;1(2):132–147. Guskiewicz KM, Marshall SW, Bailes J, et al. Neurosurgery. 2005;57(4):719–726.
6. Tripathi PN, Srivastava P, Sharma P, et al. Bioorg Chem. 2019;85:82–96. Srivastava P, Tripathi PN, Sharma P, et al. Eur J Med Chem. 2019;163:116–135.
7. Etcheberrigaray R, Alkon DL: Methods for Alzheimer's Disease treatment and cog- nitive enhancement. In: United States Patent. Edited by Patent U. USA: Blanchette Rockefeller Neurosciences Institute, Morgantown, WV; 2004.
8. Shrivastava SK, Sinha SK, Srivastava P, et al. Bioorg Chem. 2018;82:211–223.
9. Kulisevsky J. Drugs Aging. 2000;16(5):365–379.
10 Sirviö J, Riekkinen Jr P, Jäkälä P, Riekkinen PJ. Prog Neurobiol. 1994;43(4–5):363–379.
11. Vogel W, Broverman DM, Draguns JG, Klaiber EL. Psychol Bull. 1966;65(6):367.
12. Sharma P, Srivastava P, Seth A, Tripathi PN, Banerjee AG, Shrivastava SK. Prog Neurobiol. 2019;174:53–89.
13. M. Goedert, M. G. Spillantini, science 2006, 314, 777–781.

14. G. Esquerda-Canals, L. Montoliu-Gaya, J. Guell-Bosch, S. Villegas, J. Alzheimer's Dis. 2017, 57, 1171–1183.
15. A. S. Association, Alzheimers& Dementia 2014, 10, e47.
16. H. Du, L. Guo, S. Yan, A. A. Sosunov, G. M. Mckhann, S. S. Yan, Proc. Natl. Acad. Sci. U. S. A. 2010, 107, 18670–18675.
17. J. Jerabek, E. Uliassi, L. Guidotti, J. Korabecny, O. Soukup, V. Sepsova, M. Hrabinova, K. Kuca, M. Bartolini, L. E. Pena-Altamira, S. Petralla, B. Monti, M. Roberti, M. L. Bolognesi, Eur. J. Med. Chem. 2017, 127, 250–262.
18. T. Liu, Z. Xia, W. W. Zhang, J. R. Xu, X. X. Ge, J. Li, Y. Cui, Z. B. Qiu, J. Xu, Q. Xie, Pharmacol., Biochem. Behav. 2013, 104, 138–143.
19. H. Sugimoto, Y. Yamanishi, Y. Iimura, Y. Kawakami, Curr. Med. Chem. 2000, 7, 303–339.
20. A. Kumar, A. Singh, Ekavali, Pharmacol. Rep. 2015, 67, 195–203.
21. U. Jagtap, M. M. Lekhak, D. P. Fulzele, S. R. Yadav, V. A. Bapt, Curr. Sci. 2014, 107, 2008–2010.
22. G. Yang, Y. Wang, J. Tian, J. P. Liu, Plos One 2013, 8, e74916.
23. B. W. Jr, G. K. Sood, D. R. Crowe, M. B. Fallon, J. Clin. Gastroenterol. 1998, 26, 57–59.
24. N. Guzior, A. Wieckowska, D. Panek, B. Malawska, Curr. Med. Chem. 2015, 22, 373–404.
24. aS.-S. Xie, J.-S. Lan, X.-B. Wang, N. Jiang, G. Dong, Z.-R. Li, K. D. Wang, P.-P. Guo, L.-Y. Kong, Eur. J. Med. Chem. 2015, 93, 42–50; bA. Wie ˛ ckowska, M. Kołaczkowski, A. Bucki, J. Godyn ´, M. Marcinkowska, K. Wie ˛ ckowski, P. Zare ˛ ba, A. Siwek, G. Kazek, M. Głuch-Lutwin, Eur. J. Med. Chem. 2016, 124, 63–81.
25. X. Yang, X. Qiang, Y. Li, L. Luo, R. Xu, Y. Zheng, Z. Cao, Z. Tan, Y. Deng, Bioorg. Chem. 2017, 71, 305–314.
26. N. Siddiqui, M. F. Arshad, W. Ahsan, M. S. Alam, Int. J. Pharm. Sci. Drug Res. 2009, 1, 136–143.
27. World Health Organization. Dementia Fact Sheet. WHO; 2023.
28. Hardy J, Selkoe DJ. The amyloid hypothesis of Alzheimer's disease: progress and problems on the road to therapeutics. Science. 2002;297(5580):353–356.
29. Birks JS, Harvey RJ. Donepezil for dementia due to Alzheimer's disease. Cochrane Database Syst Rev. 2018;6:CD001190.
30. Knopman DS, Jones DT, Greicius MD. Failure to demonstrate efficacy of aducanumab: An analysis of the EMERGE and ENGAGE trials as reported by Biogen. Alzheimers Dement. 2021;17(4):696–701.
31. Khalafi-Nezhad A, et al. Synthesis and pharmacological evaluation of 1,2,4-triazine derivatives as novel anticholinesterase agents. Eur J Med Chem. 2014;75:47–53.
32. Nisar M, et al. Synthesis of 1,2,4-triazine derivatives and their biological activities. Bioorg Med Chem Lett. 2012;22(8):2671–2674.
33. Yi Y, et al. Triazine derivatives as multifunctional AChE inhibitors: Design, synthesis, and biological evaluation. MedChemComm. 2015;6(4):721–727.
34. Prakash O, Kumar R, Sharma N. Oxazole: A privileged heterocyclic scaffold in medicinal chemistry. Curr Med Chem. 2020;27(26):4297–4321.
35. Mukherjee S, et al. Oxazole derivatives and their therapeutic importance: A review. Eur J Med Chem. 2019;167:269–301.
36. Kwon Y. Therapeutic strategies for Alzheimer's disease: A review of recent developments. Neurotherapeutics. 2022;19(2):473–489.
37. Kumar D, et al. Design and synthesis of novel triazine derivatives with CNS activity. Bioorg Med Chem Lett. 2013;23(22):6281–6285.
38. Silva R, et al. Molecular hybridization strategies in the development of multitarget Alzheimer's disease drugs. Eur J Med Chem. 2020;192:112182.
39. Anand P, Singh B. A review on cholinesterase inhibitors for Alzheimer's disease. Arch Pharm Res. 2013;36(4):375–399.
40. Lipinski CA. Lead- and drug-like compounds: The rule-of-five revolution. Drug Discov Today Technol. 2004;1(4):337–341.
41. G.L. Ellman, K.D. Courtney, V. Andres Jr, R.M. Featherstone, A new and rapid colorimetric determination of acetylcholinesterase activity, Biochem. Pharmacol. 7 (2) (1961) 88–95.